Physics Letters B 755 (2016) 475–480

Contents lists available at ScienceDirect

Physics Letters B

www.elsevier.com/locate/physletb

Probing clustering in excited alpha-conjugate nuclei

B. Borderie [a,*], Ad.R. Raduta [a,b], G. Ademard [a], M.F. Rivet [a,1], E. De Filippo [c], E. Geraci [c,d,e], N. Le Neindre [a,f], R. Alba [g], F. Amorini [g], G. Cardella [c], M. Chatterjee [h], D. Guinet [i], P. Lautesse [i], E. La Guidara [c,j], G. Lanzalone [g,k], G. Lanzano [c,1], I. Lombardo [g,l], O. Lopez [f], C. Maiolino [g], A. Pagano [c], M. Papa [c], S. Pirrone [c], G. Politi [c,d], F. Porto [g,d], F. Rizzo [g,d], P. Russotto [g,d], J.P. Wieleczko [m]

[a] Institut de Physique Nucléaire, CNRS/IN2P3, Univ. Paris-Sud, Université Paris-Saclay, Orsay, France
[b] National Institute for Physics and Nuclear Engineering, Bucharest-Magurele, Romania
[c] INFN, Sezione di Catania, Italy
[d] Dipartimento di Fisica e Astronomia, Università di Catania, Italy
[e] INFN, Sezione di Bologna and Dipartimento di Fisica, Università di Bologna, Italy
[f] LPC, CNRS/IN2P3, Ensicaen, Université de Caen, Caen, France
[g] INFN, Laboratori Nazionali del Sud, Catania, Italy
[h] Saha Institute of Nuclear Physics, Kolkata, India
[i] Institut de Physique Nucléaire, CNRS/IN2P3, Univ. Claude Bernard Lyon 1, Université de Lyon, Villeurbanne, France
[j] CSFNSM, Catania, Italy
[k] Facoltá di Ingegneria e Architettura, Università Kore, Enna, Italy
[l] Dipartimento di scienze Fisiche, Università Federico II and INFN, Sezione di Napoli, Italy
[m] GANIL, DSM-CEA/CNRS/IN2P3, Caen, France

ARTICLE INFO

Article history:
Received 10 December 2015
Received in revised form 22 February 2016
Accepted 25 February 2016
Available online 2 March 2016
Editor: V. Metag

Keywords:
Heavy ion reactions
alpha-particle clustering
alpha-conjugate nuclei
Cluster models

ABSTRACT

The fragmentation of quasi-projectiles from the nuclear reaction ^{40}Ca+^{12}C at 25 MeV per nucleon bombarding energy was used to produce α-emission sources. From a careful selection of these sources provided by a complete detection and from comparisons with models of sequential and simultaneous decays, evidence in favor of α-particle clustering from excited ^{16}O, ^{20}Ne and ^{24}Mg is reported.

Clustering is a generic phenomenon which can appear in homogeneous matter when density decreases; the formation of galaxies as well as the disintegration of hot dilute heavy nuclei into lighter nuclei are extreme examples occurring in nature. As far as nuclear physics is concerned, the nucleus viewed as a collection of α-particles was discussed very early [1] and in the last forty years both theoretical and experimental efforts were devoted to the study of clustering phenomena in nuclei [2–4]. It was recently shown clear deviations from statistical models in the decay pattern of excited ^{24}Mg nuclei: measured emission channels involving multiple α-particles are 20 to 40% more probable than expected [5–7]. It is also known that low density nuclear matter is predicted to be unstable against cluster formation, mainly α-particles [8,9], and that excited states of alpha-conjugate nuclei like ^{12}C and ^{16}O are well described assuming a weakly interacting gas of almost free α-particles, which can be qualified as an α-particle condensate state [10,11]. Very recently the formation of α-particle clustering from excited expanding alpha-conjugate nuclei was revealed in two different constrained self-consistent mean field calculations [12,13].

The aim of the present Letter is to search for experimental evidence of α-particle clustering from excited and consequently expanding alpha-conjugate nuclei. The chosen experimental strategy was to use the reaction ^{40}Ca+^{12}C at an incident energy (25 MeV

* Corresponding author.
E-mail address: borderie@ipno.in2p3.fr (B. Borderie).
[1] Deceased.

http://dx.doi.org/10.1016/j.physletb.2016.02.061

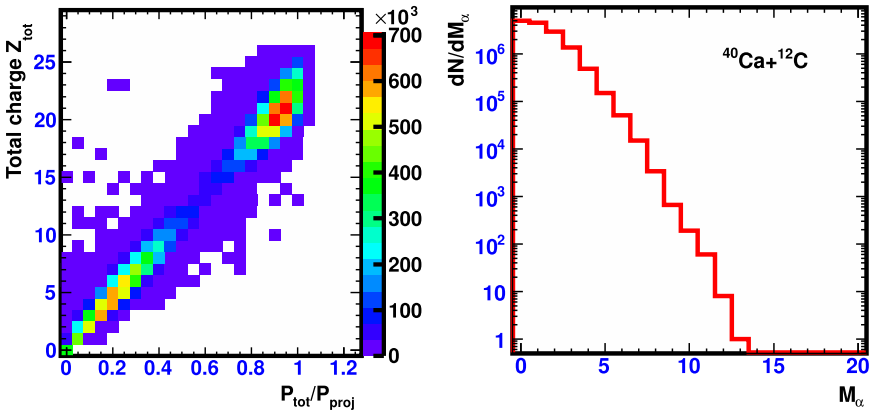

Fig. 1. (Color online.) Left: contour plot showing event-by-event correlations between the total detected charge Z_{tot} and the normalized pseudo linear momentum (see text). Right: distribution of α-particle multiplicity, M_α, for well detected events ($Z_{tot} \geq 19$).

per nucleon) high enough to possibly produce some hot expanding reaction products, associated with a high granularity, high solid angle particle array (to precisely reconstruct directions of velocity vectors). Then, by selecting the appropriate reaction mechanism and specific events, the required information was inferred.

The experiment was performed at INFN, Laboratori Nazionali del Sud in Catania, Italy. The beam, impinging on a thin carbon target (320 μg/cm^2), was delivered by the Superconducting Cyclotron and the charged reaction products were detected by the CHIMERA 4π multi-detector [14]. The beam intensity was kept around 10^7 ions/s to avoid pile-up events. Events were registered when the silicon detectors of at least three telescopes were fired. CHIMERA consists of 1192 telescopes made of ΔE silicon detectors 200–300 μm thick (depending on polar angle) and CsI(Tl) stopping detectors. They are mounted on 35 rings covering 94% of the solid angle, with polar angle ranging from 1° to 176°. The solid angle corresponding to each module varies between 0.13 msr at forward angles and 35.4 msr at the most backward angles. Among the most interesting characteristics of CHIMERA are the low detection and identification thresholds for light charged particles (LCPs) and the very high granularity at forward angles. Mass A and charge number Z of detected reaction products were determined by the energy vs time-of-flight method (TOF) for LCPs stopped in silicon detectors and by $\Delta E - E$ ($Z > 5$) and shape identification ($Z \leq 5$) techniques for charged products stopped in CsI(Tl). In addition, part of emitted ^{8}Be nuclei (two equal-energy α's hitting the same crystal) were identified in CsI(Tl) [15]. Silicon detectors were calibrated using proton, carbon and oxygen beams at various energies ranging from 10 to 100 MeV and energy measured with a resolution better than 1%. As α-particles of interest lose the major part of their energy in CsI(Tl) crystals, a dedicated energy calibration of their fast component light was realized using the TOF information and more than 95% of modules from 1° to 62° were calibrated. The energy resolution for alpha particles varies between 1.0 and 2.5% depending on the module. Further details on A and Z identifications and on the quality of energy calibrations can be found in Refs. [16–18]. In the present work, all reaction products hitting a detection module were considered as emitted in direction of the geometrical center of that module (see [18] for this choice). When results of simulations were filtered by the multi-detector replica, the same prescription was applied.

As a first step in our event selection procedure, we want to exclude from the data sample poorly-measured events. Without making any hypothesis about the physics of the studied reaction one can measure (see Fig. 1 (left)) the total detected charge Z_{tot} (neutrons are not measured) and the total pseudo linear momentum normalized to the projectile momentum P_{tot}/P_{proj} (see Eq. (1))

$$P_{tot} = \sum \beta_{par} \gamma Z. \tag{1}$$

β_{par} is the reduced velocity component, with respect to the beam direction, of the reaction product of atomic number Z and γ is the Lorentz factor. As the grazing angle of the reaction is 1.11°, to suppress elastic and quasi-elastic reactions, the first internal ring (1.0°–1.8° polar angle) of CHIMERA was removed to obtain the data in Fig. 1 (left). Well measured events clearly appear in the upper right part of the figure. In relation with their cross-sections and with the geometrical efficiency of CHIMERA, the well detected reaction mechanisms correspond to projectile fragmentation (PF) [19–21] with $Z_{tot} = 19$–20 (target fragmentation not detected) and to incomplete/complete fusion [22] with $Z_{tot} = 21$–26. At this stage we can have a first indication of the multiplicity of α-particles, M_α, emitted per event for well identified mechanisms ($Z_{tot} \geq 19$ – see Fig. 1 (right)). M_α extends up to thirteen, which means a deexcitation of the total system into α-particles only. Moreover a reasonable number of events exhibit M_α values up to about 6–7.

The goal is now to tentatively isolate, in events, reaction products emitting α-particles only. Ref. [19] has shown that, at an incident energy close to ours, ^{20}Ne PF is dominated by alpha-conjugate reaction products. Based on this, and expecting the same for ^{40}Ca PF, we restrict our selection to completely detected ($Z_{tot} = 20$) PF events composed of one projectile fragment and α-particles. Charge conservation imposes $Z_{frag} = 20 - 2M_\alpha$. Fig. 2 shows an example of the mass number distribution, A_{frag}, for $Z_{frag} = 8$ associated to $M_\alpha = 6$. As expected $A_{frag} = 16$ largely dominates; only about 8% of events correspond to neutron transfers between projectile and target and lead to an A_{frag} which is different from sixteen.

After this double selection, the question is: from which emission source are the α-particles emitted? Several possible candidates are present and further selections must be done before restricting our study to alpha-sources emitting exclusively the M_α observed (called $N\alpha$ sources in what follows). Possibilities that we shall examine concern: i) pre-equilibrium (PE) α-particle emission, ii) PF deexcitation through α-particle emission proceeding via unbound states and iii) evaporation from excited Ca projectiles having emitted α-particles only. Concerning deexcitation of PF events via unbound states, we want, for instance, to exclude from the selection an event composed of two fragments (^{24}Mg and ^{12}C*) and one α-particle finally producing one fragment (^{24}Mg) and four α-particles.

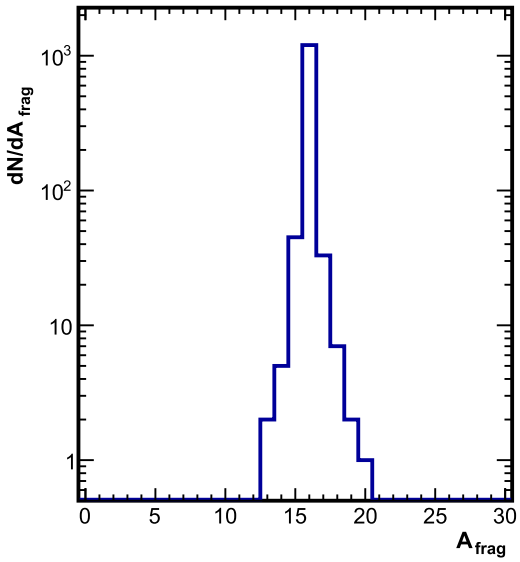

Fig. 2. (Color online.) Fragment mass number (A_{frag}) distribution associated with selected events ($Z_{tot} = 20$) where $Z_{frag} = 8$ and $M_\alpha = 6$.

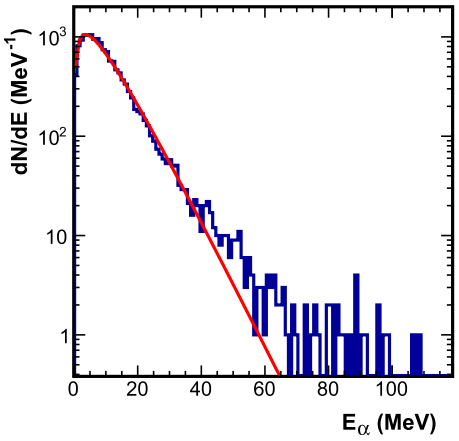

Fig. 3. (Color online.) α-particles emitted by $M_\alpha = 5$ events: energy spectrum in the N_α reference frame; curve corresponds to a Maxwellian fit (see text).

Considering the incident energy of the reaction and the forward focusing of reaction products, it is important to identify the possible presence of pre-equilibrium (PE) α-particles [23–25] in our selected PF events. With the hypothesis that all α-particles are emitted from their center-of-mass reference frame, we can examine the corresponding α-particle spectra. Fig. 3 shows one example of such spectra for $M_\alpha = 5$. It exhibits a distribution which resembles a thermal one with the presence of a high energy tail, which signs PE emission; a similar spectrum, in the center-of-mass of the reaction, is obtained at forward angles for the involved collisions. To prevent errors on alpha emitter properties it is necessary to remove events in which such PE emission can be present. The curve superimposed on the spectrum in Fig. 3 corresponds to a thermal Maxwellian fit (Coulomb correction, C_c, of 0.22 MeV and temperature, T, of 6.5 MeV) with a volume pre-exponential factor: $dN/dE \propto (E - C_c)^{1/2} \exp[-(E - C_c)/T]$ [26]. It was used to impose an upper energy limit of 40 MeV, found irrespective of M_α, for α-particles. Table 1 displays the percentages of suppressed events.

As far as deexcitation of selected PF events via unbound states is concerned the use of multi-particle correlation functions (MCFs) [27] is required to suppress events. Correlation function is defined as the ratio between the correlated (physical) yield, Y_{corr},

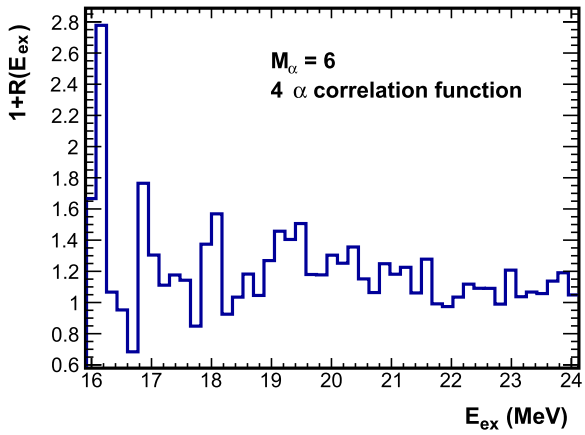

Fig. 4. (Color online.) α-particles emitted by $M_\alpha = 6$ events: four α-particle correlation function as a function of excitation energy.

Table 1
Information on selected events with different α multiplicities, M_α: percentages of suppressed events containing pre-equilibrium α-particle emission (PE), excited α sub-systems (see text) and final number of selected events. Percentages in parentheses correspond to statistical errors.

	PE α-emission	Excited α sub-systems	
M_α	suppressed events (%)	suppressed events (%)	final number of selected events
4	6.9 (0.2)	1.6 (0.1)	12780
5	7.1 (0.5)	3.1 (0.3)	2623
6	9.2 (0.8)	3.6 (0.5)	1129
7	8.7 (1.6)	3.9 (1.1)	291

and the product of single particle yields, generically termed as uncorrelated spectrum, Y_{uncorr}, measured under the same conditions,

$$1 + R(X) = \frac{Y_{corr}(X)}{Y_{uncorr}(X)}. \quad (2)$$

The correlated yield spectrum Y_{corr} is constructed with the required number of α-particles detected in the same event and we choose to build Y_{uncorr} by mixing particles from different events [28]. If no correlations are present MCF should be unity. The generic variable X is the total kinetic energy of the particles of interest in their center-of-mass frame, E_{tot}, or the excitation energy of their emitting source/state, $E_{ex} = E_{tot} + Q$; Q is the mass balance. As an example, for events with $M_\alpha = 6$ we build three-, four- and five-particle MCFs considering all possible combinations of α-particles. Fig. 4 displays the four-particle MCF. Peaks, statistically significant, are located in the excitation energy range 16.7–22.0 MeV. Considering the experimental resolution measured, around 350 keV [18], the following peaks or sum of two peaks which correspond to unbound states of ^{16}O are observed: 16.84 + 17.20, 17.72 + 18.09, 19.26 + 19.54, 20.05 + 20.41, 21.05 and 21.65 MeV; some of them 16.84 and 21.05 being known as 100% α-particle emitters. This is a clear indication that some deexcitation via those states occurs. From those MCF studies it appears that only two nuclei, ^{12}C (Hoyle state and broad peak centered at 9.64 MeV excitation energy) and ^{16}O (see Fig. 4) significantly contribute to deexcitation via their unbound states. For each M_α value, average MCF values corresponding to each state have been calculated and only a percentage of events (from 1 to 95%) with α-particles populating those states were kept. Percentages kept correspond to the weights (in percent) of background levels under the peaks: $1 - [(\text{MCF} - 1)/\text{MCF}] = 1/\text{MCF}$. Table 1 shows the small percentages of suppressed events (from 1.6 to 3.9%), which obviously concern events with low energy α-particles

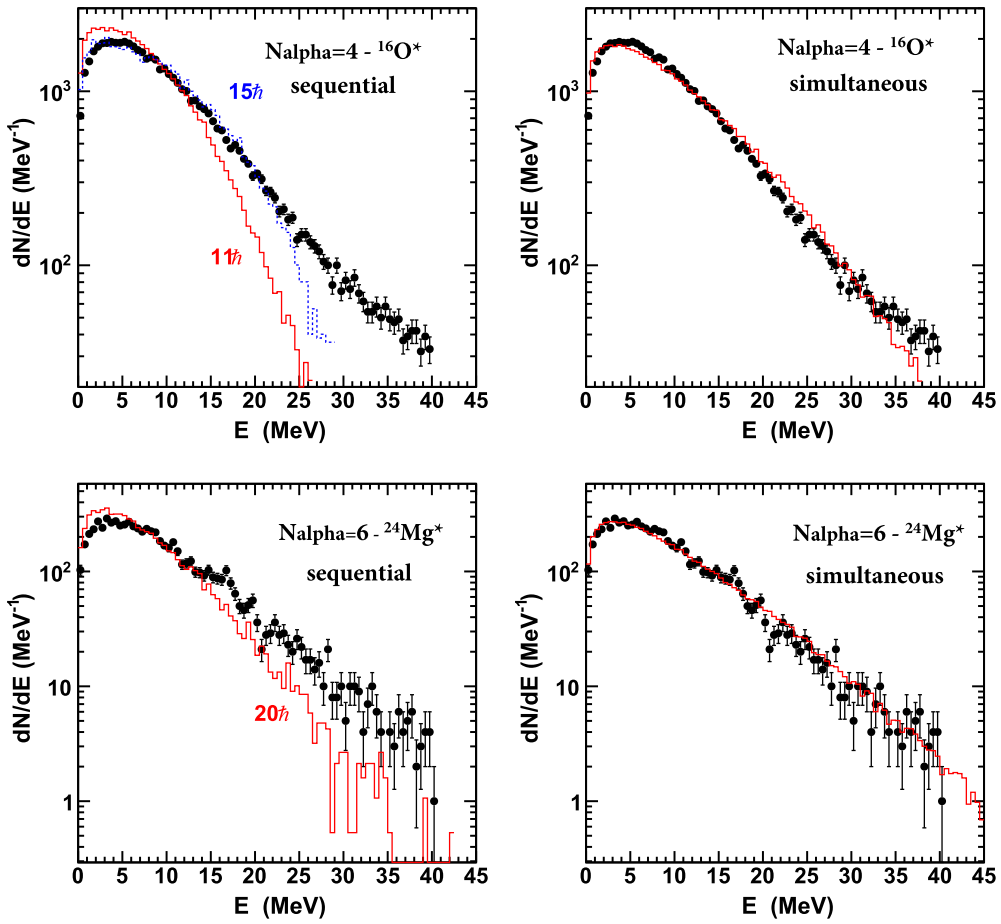

Fig. 5. (Color online.) Particle spectra from $N\alpha$ sources: ^{16}O*, top and ^{24}Mg*, bottom; black dots with statistical error bars correspond to experimental data. Histograms superimposed on data correspond to filtered simulations: left – for sequential decay and different spin distributions with GEMINI++ and right – with a dedicated simulation of a simultaneous decay process (see text).

in their α reference frame. Final numbers of selected events for each of the M_α values are also indicated, which show sufficient statistics for comparisons with simulations for $M_\alpha = 4$–6.

As far as $N\alpha$ sources are concerned, the effect of suppressing events is to reduce both the mean values and the widths of their excitation energy distributions. As an example, for $N\alpha = 4$, mean excitation decreases from 56.2 to 52.4 MeV and the root mean square (RMS) of the distribution from 22.7 to 15.7 MeV. The corresponding α-energy spectrum (top, black dots) is displayed in Fig. 5; for comparison same information is also reported for $N\alpha = 6$ (bottom, black dots). For deduced excitation energies we did not consider deexcitations via ^{8}Be because they do not significantly modify the conclusions. However, for completeness, Table 2 shows the percentages of one and two ^{8}Be emissions measured from relative energy spectra of two α-particles and associated correlation functions for different M_α values; percentages with three ^{8}Be are found negligible (<1%). Information relative to ^{8}Be emission will be important to discuss sequential versus simultaneous α-emission from $N\alpha$ sources.

To conclude on this part, one can indicate that if excited $N\alpha$ sources have been formed their excitation energy thresholds for total deexcitation into α-particles vary from 20 to 50 MeV as $N\alpha$ varies from 4 to 6. Their mean excitation energy per nucleon is rather constant around 3.3–3.5 MeV. One can also deduce a crude estimation of the average lowest density they may have reached due to thermal pressure before decaying into α-particles. To do that, starting from a phenomenological quadratic equation of state

Table 2
Percentages of selected events which deexcite via one or two ^{8}Be as a function of α multiplicity M_α; percentages in parentheses correspond to statistical errors. Results from GEMINI++ simulations for $N\alpha$ sources are also reported.

M_α	Selected events		GEMINI++ results	
	one ^{8}Be	two ^{8}Be	one ^{8}Be	two ^{8}Be
4	7.7 (0.3)	0.2	100.0	0.0
5	12.0 (0.7)	0.2	59.4	40.6
6	19.3 (1.3)	0.4	13.5	86.5

(EoS) [29], an EoS for subnormal density of finite nuclear systems was proposed in [30]:

$$(E/A)_{T=0} = 8[(1-\rho/\rho_0)^2 - 1]\ \text{MeV}. \quad (3)$$

From Eq. (3) introducing an initial excitation energy at normal density and ignoring any dissipative processes during the expansion stage (excitation energy = expansion energy) an estimation of the minimum density reached can be calculated [31]. The minimal average density ρ which was derived is found around $0.7\rho_0$ where ρ_0 is the normal density.

Before discussing different possible deexcitations involved for final retained events, information on projectile fragmentation mechanism is needed. Global features of PF events are reproduced by a model of stochastic transfers [21]. Main characteristics for primary events with $Z_{tot} = 20$ are the following: i) excitation energy extends up to about 200 MeV, which allows the large excitation energy domain (20–150 MeV) measured for $N\alpha$ sources when associated to a single fragment, and ii) angular momenta extend up

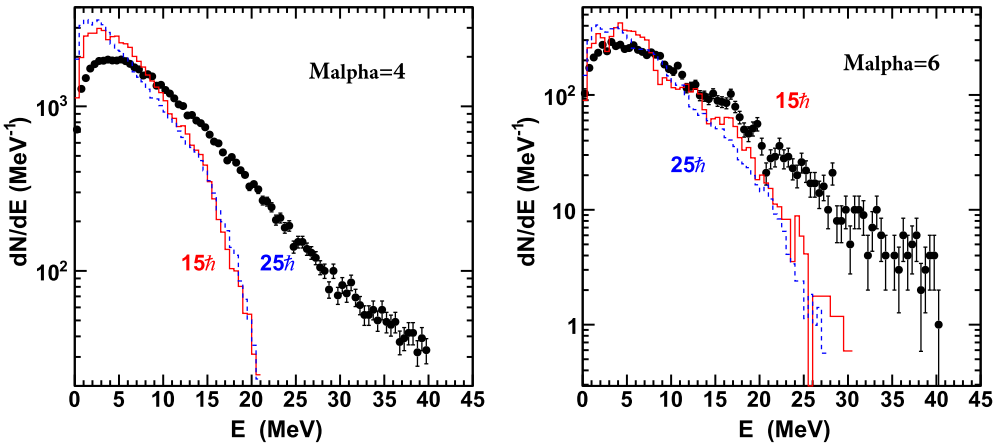

Fig. 6. (Color online.) Sequential decay of excited Ca projectiles: energy spectra (in the $M_\alpha = 4$ (left) or $M_\alpha = 6$ (right) system reference frame) of evaporated α-particles associated to a ^{24}Mg (left) or to an ^{16}O (right) evaporation residue. Black dots are experimental data and histograms are results of GEMINI++ simulations (see text).

to 24$\hbar$, which gives an upper spin limit for excited Ca projectiles and consequently for $N\alpha$ sources.

Are α-particles emitted sequentially or simultaneously? To answer the question α-energy spectra can be compared to simulations. For excited Ca projectiles and $N\alpha$ sources, experimental velocity and excitation energy distributions as well as distributions for spins are used as inputs. Results of simulations are then filtered by the multi-detector replica including all detection and identification details. Simulated spectra are normalized to the area of experimental spectra.

For sequential emission the GEMINI++ code [32,33] was used. It combines the Hauser–Feshbach formalism for evaporation of particles ($Z < 5$) and the transition-state formalism for intermediate-mass fragment emission ($Z \geqslant 5$). Evaporation includes n, p, d, t, ^{3}He, α-particles, ^{6}He, $^{6-8}$Li and $^{7-10}$Be channels. For fragment emission, the saddle conditional energy for different mass (or charge) asymmetries is deduced from the finite range rotating liquid-drop model [34]. Note that emitted ^{8}Be are directly transformed into two α-particles.

Before discussing decays of $N\alpha$ sources, we must consider the possible evaporation from Ca projectiles as stated previously. Excitation energy for projectiles is deduced from $E^* = E^*(N\alpha) + E_{rel} + Q$. E_{rel} is the relative energy between the $N\alpha$ source and the associated fragment (evaporation residue). Fig. 6 (left) displays, for $M_\alpha = 4$, results of simulations (histograms) with reconstructed excitation energy distribution for ^{40}Ca ($< E^* > = 68.8$ MeV) and gaussian distributions centered at 15 and 25$\hbar$ for spins as inputs. $M_\alpha = 4$ and ^{24}Mg residues are the decay products after filtering. A similar comparison is displayed in Fig. 6 (right) for $M_\alpha = 6$; excitation energy distribution for ^{40}Ca is centered at $< E^* > =$ 99.7 MeV. RMSs used for spin distributions, around 2.0–2.5$\hbar$, were deduced from the correlation "excitation energy–spin" obtained with the model of stochastic transfers [21]. Note that no more ^{24}Mg, ^{20}Ne or ^{16}O residues are produced in simulations for ^{40}Ca spin distributions centered at values larger than 25$\hbar$. Comparisons with experimental data (full points) show a poor agreement indicating that such an hypothesis of sequential decay from excited projectiles is not correct. The same conclusion is derived for M_α equal 5 [35].

Considering sequential deexcitation of $N\alpha$ sources, histograms in Fig. 5 (left) are examples of GEMINI++ simulation results for $N\alpha = 4$ (^{16}O*) and for $N\alpha = 6$ (^{24}Mg*). Gaussian distributions for spins are used as inputs and the best agreement with data is obtained with RMS = 1.5$\hbar$ for spin distributions. The agreement between data and simulations becomes progressively poorer as the $N\alpha$ value decreases. However, the most important disagreement between data and simulations concerns the percentages of $N\alpha$ sources which deexcite via ^{8}Be (see Table 2). With the excitation energy distributions experimentally deduced the GEMINI++ code evaporates an important percentage of ^{8}Be along the deexcitation chain and at the last evaporation step of the chain leaving an unstable ^{8}Be residue. This strong constraint is not experimentally observed.

For simultaneous emission from $N\alpha$ sources, a dedicated simulation was done which mimics a situation in which α clusters are early formed when the $N\alpha$ source is expanding [12,13] due to thermal pressure. By respecting the experimental excitation energy distributions of $N\alpha$ sources, a distribution of $N\alpha$ events is generated as starting point of the simulation. Event by event, the $N\alpha$ source is first split into α's. Then the remaining available energy ($E^* + Q$) is directly randomly shared among the α-particles such as to conserve energy and linear momentum [36]. Histograms in Fig. 5 (right) are the results of such a simulation, which show a good agreement with data. Similar calculated energy spectra were also obtained with simulations containing an intermediate freeze-out volume stage where α-particles are formed and then propagation of particles in their mutual Coulomb field. In this case angular momentum distributions of $N\alpha$ sources at freeze-out can also be deduced: they exhibit a Maxwell-like shape extending up to 25$\hbar$ for $N\alpha = 6$ while mean values vary from 6.7 to 9.5$\hbar$ when $N\alpha$ moves from 4 to 6. Note that ^{8}Be emission is out of the scope of the present simulation.

From these comparisons with both sequential and simultaneous decay simulations it clearly appears that sequential emission is not able to reproduce experimental data whereas a remarkable agreement is obtained when an α-clustering scenario is assumed. Same conclusion is derived for $N\alpha$ equal 5 [35]. However one cannot exclude that a small percentage of $N\alpha$ sources, those produced with lower excitation energies, sequentially deexcite.

In conclusion, the reaction ^{40}Ca+^{12}C at 25 MeV per nucleon bombarding energy was used to produce and carefully select specific classes of projectile fragmentation events from which excited $N\alpha$ sources can be unambiguously identified. Their excitation energy distributions are derived with mean values around 3.4 MeV per nucleon and a crude estimation of their mean minimal densities, around 0.7 the normal density, can be deduced.

Their energetic emission properties were compared with two simulations, one involving sequential decays and a second for simultaneous decays. For excited expanding $N\alpha$ sources composed of 4, 5 and 6 α-particles, for which statistics is good enough for conclusive comparisons with simulations, evidence in favor of si-

multaneous emission (α-particle clustering) is reported. Those results support mean field calculations of Refs. [12,13].

References

[1] Discussion on the structure of atomic nuclei, Proc. R. Soc. Lond. A 136 (1929) 386.
[2] C. Beck (Ed.), Clusters in Nuclei, vol. 1, Lecture Notes in Physics, vol. 818, 2010, and references therein.
[3] C. Beck (Ed.), Clusters in Nuclei, vol. 2, Lecture Notes in Physics, vol. 848, 2012, and references therein.
[4] C. Beck (Ed.), Clusters in Nuclei, vol. 3, Lecture Notes in Physics, vol. 875, 2014, and references therein.
[5] G. Baiocco, et al., Phys. Rev. C 87 (2013) 054614.
[6] L. Morelli, et al., J. Phys. G.: Nucl. Part. Phys. 41 (2014) 075107.
[7] L. Morelli, et al., J. Phys. G.: Nucl. Part. Phys. 41 (2014) 075108.
[8] G. Röpke, A. Schnell, P. Schuck, P. Nozieres, Phys. Rev. Lett. 80 (1998) 3177.
[9] M. Beyer, S.A. Sofianos, C. Kuhrts, G. Röpke, P. Schuck, Phys. Lett. B 448 (2000) 247.
[10] A. Tohsaki, H. Horiuchi, P. Schuck, G. Röpke, Phys. Rev. Lett. 87 (2001) 192501.
[11] Y. Funaki, T. Yamada, H. Horiuchi, G. Röpke, P. Schuck, A. Tohsaki, Phys. Rev. Lett. 101 (2008) 082502.
[12] M. Girod, P. Schuck, Phys. Rev. Lett. 111 (2013) 132503.
[13] J.P. Ebran, E. Khan, T. Nikšić, D. Vretenar, Phys. Rev. C 89 (2014) 031303(R).
[14] A. Pagano, et al., Nucl. Phys. A 734 (2004) 504.
[15] L. Morelli, et al., Nucl. Instrum. Methods A 620 (2010) 305.
[16] M. Alderighi, et al., Nucl. Instrum. Methods Phys. Res. A 489 (2002) 257.
[17] N. Le Neindre, et al., Nucl. Instrum. Methods Phys. Res. A 490 (2002) 251.
[18] Ad.R. Raduta, et al., Phys. Lett. B 705 (2011) 65.
[19] M. Morjean, et al., Nucl. Phys. A 438 (1985) 547.
[20] B. Borderie, M.F. Rivet, L. Tassan-Got, Ann. Phys. Fr. 15 (1990) 287.
[21] L. Tassan-Got, C. Stephan, Nucl. Phys. A 524 (1991) 121.
[22] P. Eudes, et al., Phys. Rev. C 90 (2014) 034609.
[23] O. Lopez, et al., INDRA Collaboration, Phys. Rev. C 90 (2014) 064602.
[24] P. Pawlowski, et al., INDRA Collaboration, Eur. Phys. J. A 9 (2000) 371.
[25] O. Fotina, et al., EPJ Web Conf. 66 (2014) 03028.
[26] A. Goldhaber, Phys. Rev. C 17 (1978) 2243.
[27] R.J. Charity, et al., Phys. Rev. C 52 (1995) 3126.
[28] M.A. Lisa, et al., Phys. Rev. C 44 (1991) 2865.
[29] H. Stöcker, W. Greiner, Phys. Rep. 137 (1986) 227.
[30] W.A. Friedman, Phys. Rev. C 22 (1990) 667.
[31] B. Borderie, in: G. Giardina, G. Fazio, M. Lattuada (Eds.), Large-Scale Collective Motion of Atomic Nuclei, World Scientific, Singapore, 1997, p. 1.
[32] R.J. Charity, Phys. Rev. C 82 (2010) 014610, and references therein.
[33] D. Mancusi, R.J. Charity, J. Cugnon, Phys. Rev. C 82 (2010) 044610, and references therein.
[34] A.J. Sierk, Phys. Rev. Lett. 55 (1985) 582.
[35] B. Borderie, et al., in: Proc. 12th Int. Conf. on Nucleus–Nucleus Collisions (NN2015), EPJ Web Conf. (2016), in press, arXiv:1602.05827.
[36] J.A. Lopez, J. Randrup, Nucl. Phys. A 491 (1989) 477.